

CHAPTER III

EXPERIMENTS AND TECHNIQUES

SiO₂ and TiO₂ single layer thin films will be deposited on glass substrates by custom-built RF magnetron sputtering of a pure SiO₂ and TiO₂ ceramic target respectively (diameter 3 inches) mm). Before each deposition, the sputtering chamber will be evacuated down to a pressure of 1×10^{-5} mbar (or lower). The film deposition carries out at room temperature. The substrate–target distance is about 15 cm. The sputtering target is continuously cooled by water. Pure argon is used as the sputtering gas and pure oxygen as the reactive gas. The effect of deposition parameters such as RF power and gas flow rate on the structural and optical properties of the samples will be studied.

The phase analysis of the prepared samples was carried out using an X-ray diffractometer. The surface morphology will be examined by SEM and AFM. XPS will be used to characterize the stoichiometry of the films and to identify the chemical state of Si and Ti atoms. The optical constants will be measured by spectroscopic ellipsometer. The optical transmittance and reflectance will be obtained by UV-Vis-NIR measurement. The local structure will be investigated by XAS. In particular, XANES gives information on oxidation state and site symmetry of Si (or Ti) and EXAFS gives detailed information on distances and coordination numbers of neighboring atom shells surrounding the Si (or Ti) atom. After getting desired optical properties of prepared single layer films and being able to control film thickness and refractive index, thin film multilayer of silicon oxide and titanium oxide materials is designed and fabricated.

3.1 Thin films preparation

3.1.1 RF Magnetron Sputter Deposition

Sputter deposition is a vacuum coating process categorized in the type of physical vapor deposition (PVD). Sputtering process is a well-known film growth technique for the coating industry.

The technique is based on ion bombardment of a source material (the target). Sputter deposition is a non-thermal vaporization process which uses a physical phenomenon to produce the microscopic spray effect. When an energetic ion strikes the surface of the target, atoms of that target material are ejected by a momentum transfer process. Sputtering working gas will be ionized and accelerated towards the target. The use of a magnetron allows trapping of the electrons by the magnetic field lines close to the sputtering target in a well-defined region. Therefore, electrons stay within the plasma for a considerably longer time, increasing the probability of ionizing the working gas. Magnetron sputtering cathodes can be run using AC or DC power supplies. The most common AC power supplies usually operate in the RF range at 13.56 MHz in order to sputter also high insulating target materials like SiO₂ or Al₂O₃ (Bräuer *et al.*, 2010).

Basically, the sputtering target is actively cooled. The cold surface minimizes the amount of radiant heat in a sputtering system and this may be an advantage over thermal evaporation in vacuums, where the radiant heat load can be appreciable. The low level of radiant heat is one factor that allows thermally sensitive surfaces to be placed near the sputtering target. Cooling also prevents diffusion in the target, which could lead to changes in the elemental composition in the surface region when alloy targets are bombarded (Mattox, Donald M., 2010).

Table 3.1 Sputtering yields by 500 eV ions (Mattox, Donald M., 2010).

	Be (9)	Al (27)	Si (28)	Cu (64)	Ag (106)	W (184)	Au (197)
He ⁺ (4amu)	0.24	0.16	0.13	0.24	0.2	0.01	0.07
Ne ⁺ (20amu)	0.42	0.73	0.48	1.8	1.7	0.28	1.08
Ar ⁺ (40amu)	0.51	1.05	0.50	2.35	2.4 – 3.1	0.57	2.4
Kr ⁺ (84amu)	0.48	0.96	0.50	2.35	3.1	0.9	3.06
Xe ⁺ (131amu)	0.35	0.82	0.42	2.05	3.3	1.0	3.01

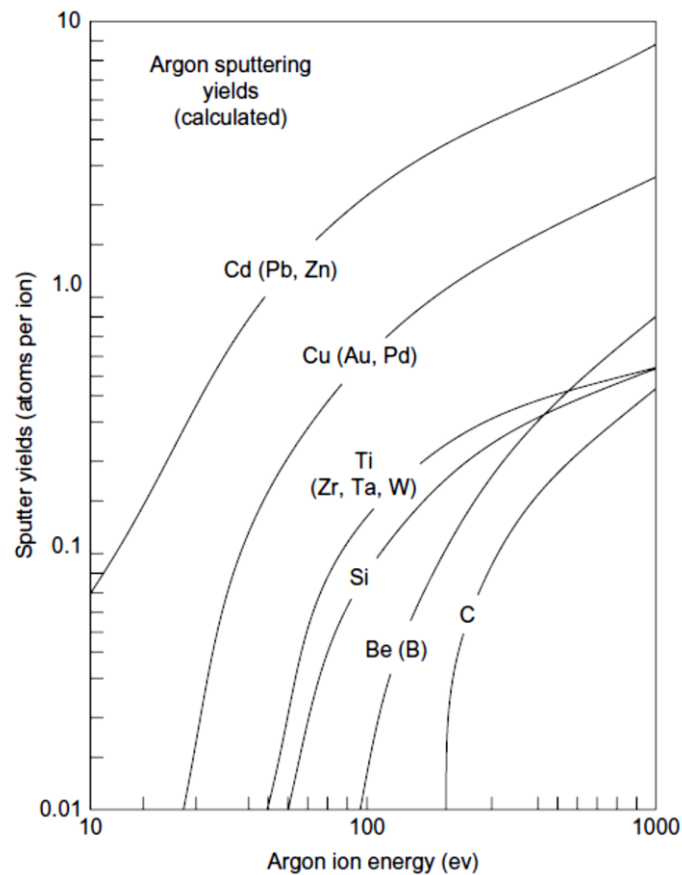


Figure 3.1 Some calculated sputtering yields (Mattox, Donald M., 2010).

The sputtering yield is the ratio of the number of atoms ejected to the number of incident bombarding particles and depends on the chemical bonding of the target atoms and the energy transferred by collision. Table 5 shows some masses of gaseous ions and target materials and the approximate sputtering yield by bombardment at the energies indicated. Figure 3.1 shows some sputtering yields by argon ion bombardment as a function of ion energy. For off-normal bombardment, the sputtering yield initially increases to a maximum then decreases rapidly as the bombarding particles are reflected from the surface; this effect is called the “angle-of-incidence effect”, as shown in Figure 3.2. The maximum sputtering yield for argon generally occurs at about 70 degrees off-normal but this varies with the relative masses of the bombarding and target species. The angle-of-incidence effect on sputtering yield, and surface mobility effects, can give rise to the development of surface features

such as cones and whiskers on the target surface. The sputtering threshold energy is a rather vague number that is the lowest energy of the bombarding particle that can cause sputtering. Generally, it is considered that incident particle energies of less than about 25 eV will not cause physical sputtering of an element. This is about the energy needed for atomic displacement in the radiation damage in solids (Mattox, 2010).

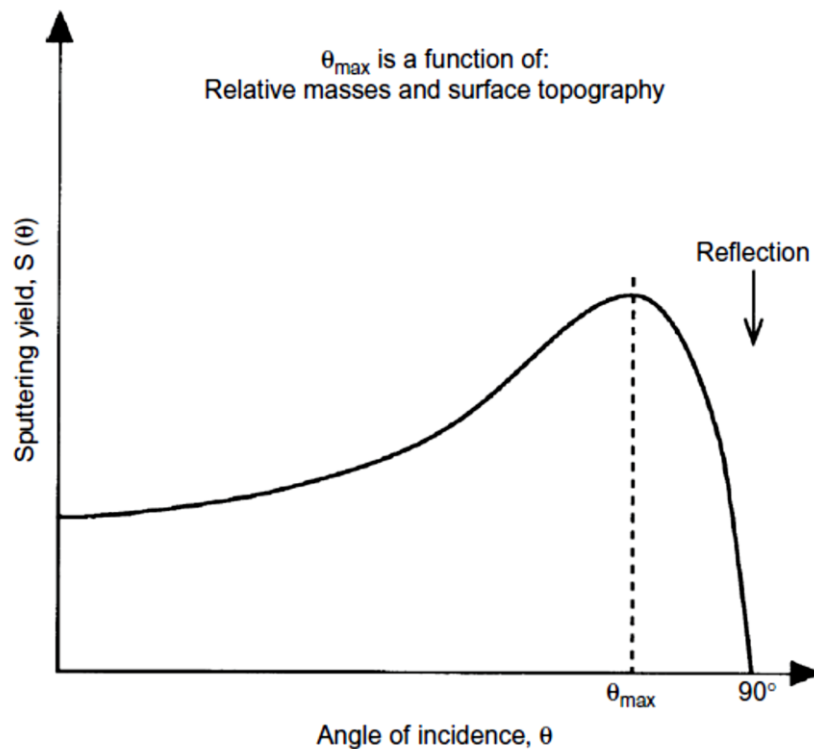


Figure 3.2 Sputtering yield as a function of angle-of-incidence of the bombarding ion (Mattox., 2010).

Magnetron sputtering emerges when a plasma is ignited in the presence of a rare gas (typically, argon) in the vicinity of the target surface. The plasma is stabilized by a magnetic field. The magnetic field thus developed traps the electrons in cycloids and keeps them circulating over the target surface in order to increase the dwell time of electrons in the gas and thereby raises the ionization probability. Magnetron sputtering sources have wide technical applications mainly in the thin film coating and processing industry. This versatile tool uses a plane solid target mounted close to an axial permanent magnet (Popok *et al.*, 2011). Schematic diagram of mechanism of magnetron sputter coating machine is shown in Figure 3.3.

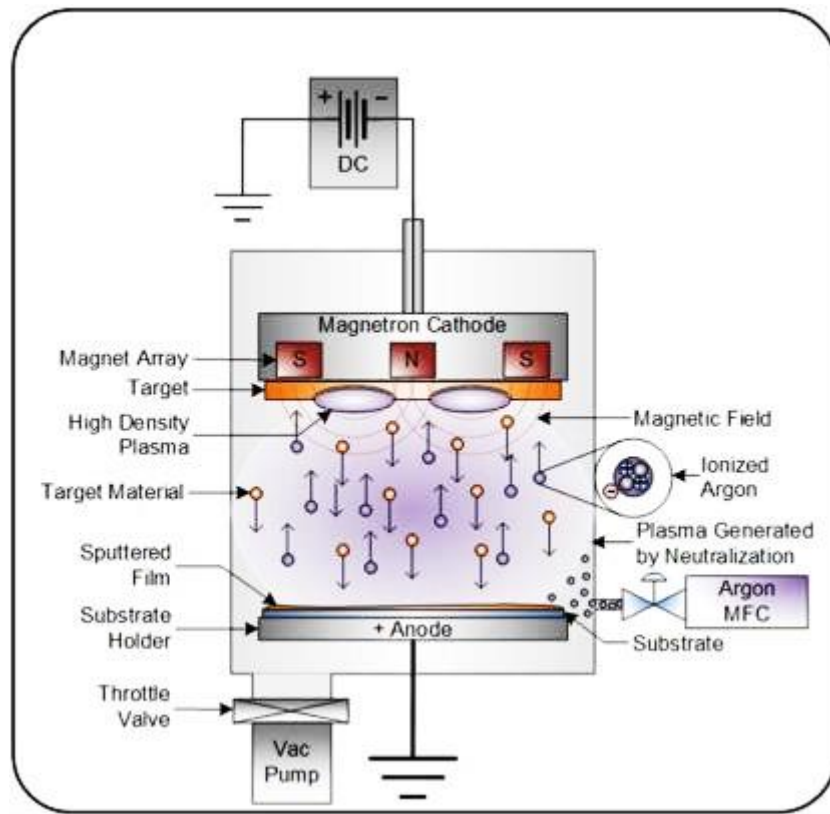


Figure 3.3 Schematic diagram of mechanism of magnetron sputter coating machine. (<https://www.sciencedirect.com/topics/materials-science/magnetron-sputtering>).

The sputtering parameters which affect the properties of the resulting films are listed below:

- The sputtering power – It influences the rate of deposition process
- The applied voltage – It determines the maximum energy of the sputtered particles ejected from the target surface and the sputtering yield.
- Sputtering gas pressure & Target- substrate distance – They control the mean free path of the sputtered particles and thereby the porosity, crystallinity and texture of the deposited thin films.
 - Reactive gas mixture – It affects the film stoichiometry.
 - Substrate temperature – It controls the density of the thin films and also the behavior of film growth with respect to crystallinity.
 - Bias-voltage to substrate – It determines the growth of the layer.

By controlling preparation conditions, the films with desired properties can be obtained from sputtering technique and it has high potential to be tunable.



Figure 3.4 RF magnetron sputtering system at BL6, SLRI.

3.1.2 Reactive Gas Timing Sputter Deposition

In the gas-timing approach, the flow of the sputtering gas is purposefully controlled via an on-and-off sequence. This technology has been used on our sputtering machine to produce high-quality crystalline thin films at ambient temperature and low RF power. Without any annealing treatment following deposition, high-quality crystalline thin films may be produced using this method (Klaitabtim, D. *et al.*, 2008). In general, the deposition rate and film characteristics are determined by the amount of reactive gas given to the system. When a film is deposited in metallic mode, the sputtering rate is high, and the resulting film is substoichiometric and rich in metallic elements. At high O_2 reactive gas in oxide mode, the film stoichiometric and deposition rate are poor because the target is covered by an oxide or nitride layer, a phenomenon known as the poisoning of sputtering target effect. To obtain both a high deposition rate and stoichiometric film, it is desirable to optimize the O_2 flow rate in transition mode. However, it was discovered that the deposition in the transition mode was unstable owing to the "hysteresis effect." The reactive gas-timing (RGT)

approach was an alternate deposition process in which the fluxes of the sputtered or reactive gases were purposefully regulated by an on-off sequence. It has been claimed that this technology successfully enhanced the standard reactive magnetron sputtering process by enabling the control of film composition at high deposition rates at low temperatures. Figure 3.5 shows Schematic representation of argon and oxygen mass flow rate versus time used for depositing TaO thin film by the conventional reactive sputtering and RGT techniques (Chittinan, D. *et al.*, 2019). The Reactive Gas Timing magnetron sputtering system at NECTEC is shown in Figure. 3.6.

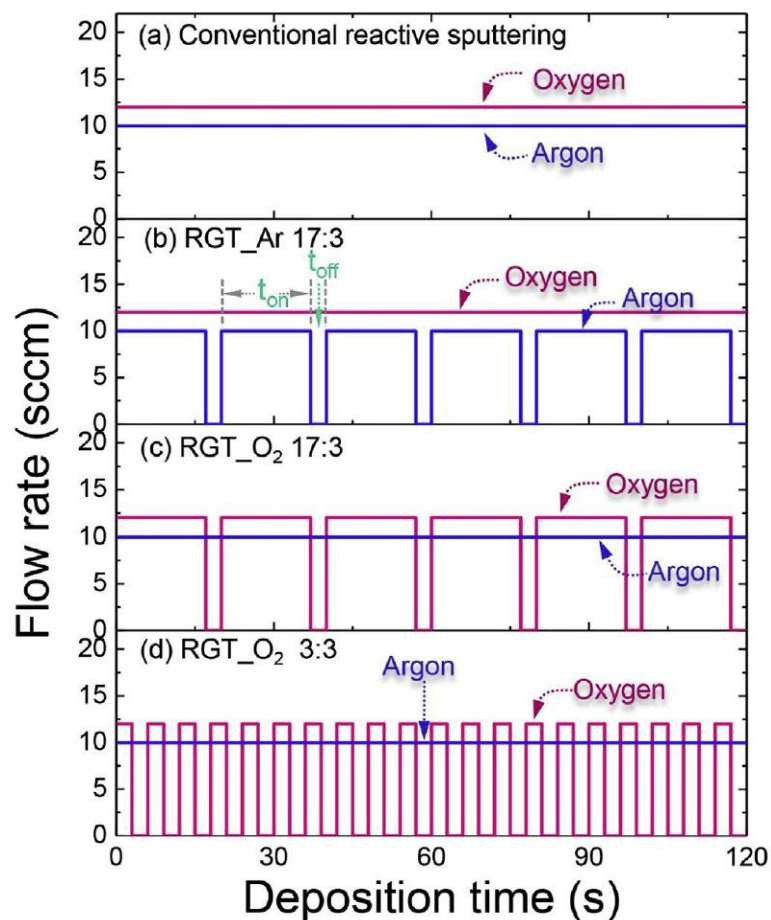


Figure 3.5 Schematic representation of argon and oxygen mass flow rate versus time used for depositing TaO thin film by the conventional reactive sputtering and RGT techniques (Chittinan, D. *et al.*, 2019).



Figure 3.6 Reactive Gas Timing magnetron sputtering system at NECTEC.

3.2 Thin films characterization techniques

Several different techniques will be used to analyze or characterize the film samples fabricated in the magnetron sputtering system. It has already been established that understanding the crystallographic phase composition, surface morphology, chemistry, and lattice defect structure is important to the research purposes for which the system was made. The importance techniques used to examine these qualities will now be summarized.

3.2.1 X-ray diffraction (XRD)

X-ray diffraction is a common material characterization technique that provides detailed information about the crystallographic structure, chemical composition, and physical properties of materials. It also allows for identification of crystal orientations and interatomic spacing ($d_{(hkl)}$). Subsequently, XRD results were showed relationship between intensity of diffraction plane peak and 2θ which come from incident X-ray direction. In plane X-ray waves, are used for this technique because wavelength is on

the same length scale as interatomic spacing and lattice parameter values. X-ray diffraction data is analyzed by using Bragg's equation (3.1) as shown in following.

For explanation of XRD equations, there are incidents' X-ray wave in the same plane that incident to atomic structure plane (s1, s2 etc.). Then, based on natural of EM wave, interval between ab+ bc = $n\lambda$ including de+ef = $m\lambda$ where n and m are counting number. Figure 3.4 showed this relationship for plan and adjacent plan. Moreover, useful trigonometry theory, we can show $\sin \theta = ab/d_{(hkl)}$, and $\sin \theta = bc/d_{(hkl)}$. For above, we will get this equation as shown in Equation 3.17.

$$n\lambda = 2d_{(hkl)}\sin\theta \quad (3.1)$$

and the angle of reflection for a particular set of lattice planes (hkl) is given as

$$2\theta = 2\sin^{-1}\left(\frac{n\lambda}{2d_{(hkl)}}\right) \quad (3.2)$$

where n is n is the order of reflection, λ is the wavelength of x-rays, $d_{(hkl)}$ is the characteristic spacing between the crystal planes of a given specimen, and θ is the angle between the incident beam and the normal to the reflecting lattice plane.

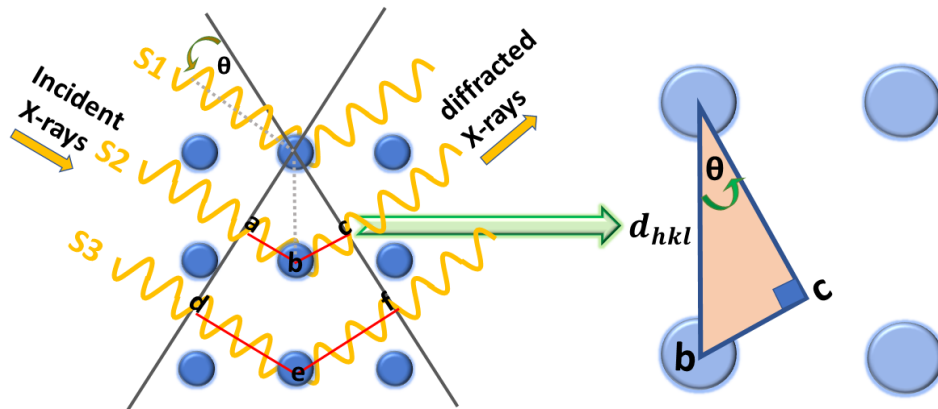


Figure 3.7 Schematic representation of Bragg's Law for XRD.

In this work, XRD measurement were performed using XRD (BRUKER, D8 ADVANCE) with Cu K_{α} radiation at a wavelength of 1.5406 Å from a generator operating at 40 kV and 40 mA.



Figure 3.8 XRD (BRUKER, D8 ADVANCE) at SUT. (<http://cste.sut.ac.th/2014/?p=1920>)

3.2.2 Scanning electron microscopy (SEM)

Scanning electron microscopy (SEM) produces images of surface sample by scanning the surface with a focused beam of electrons as shown in Figure 3.9. The principle of SEM is based on the interaction between an incident electron and the solid specimen. This interaction can produce signals that contain information about the surface topography and elemental composition of the sample. SEM images are produced by collecting two types of electrons which are backscattered electrons (BSE) and secondary electrons (SE). The secondary electrons are originated from atoms on sample surface that interact as inelastic collision with the electron beam. On the other hand, the backscattered electrons are the primary electrons which are reflected after elastic interactions between the electron beam and atoms. They are originated from deeper regions of sample surface. The BSE and SE carry different types of information. BSE image is highly sensitive to differences in atomic number such that the higher the atomic number and the brighter the material appears in the image, while SE image can provide more detailed surface information.

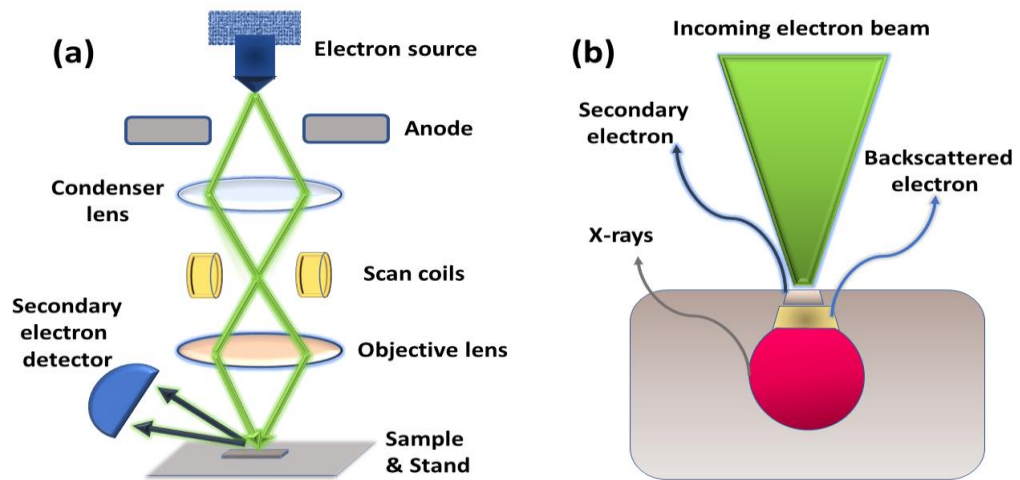


Figure 3.9 Schematic diagram of (a) basic SEM components and (b) different types of SEM signals.

In this study, SEM image were provided using SEM machine from Zeiss AURIGA FE-SEM/FIB/EDX located at SUT.



Figure 3.10 SEM machine (Zeiss AURIGA) located at SUT(<http://cste.sut.ac.th/>).

3.2.3 X-ray Absorptions Spectroscopy (XAS)

X-ray absorption spectroscopy (XAS) measures the energy-dependent fine structure of the X-ray absorption coefficient near the absorption edge of a particular element. From XAS principle, electron was ejected by x-ray source which enough energy for exciting. A typical XAS System is mainly divided into two parts simply input system and output system. Input is electron gas ionized signal at incident chamber (I_0). Output is electron ionized signal at transmitted chamber (I_t). The electron X-ray absorptions can be explaining by following equations:

$$\mu x = \ln(I_0/I_t) \quad (3.3)$$

Where: μ is transmission coefficient
 x is thickness of film
 I_0 is incident light intensity
 I_t is transmitted light intensity

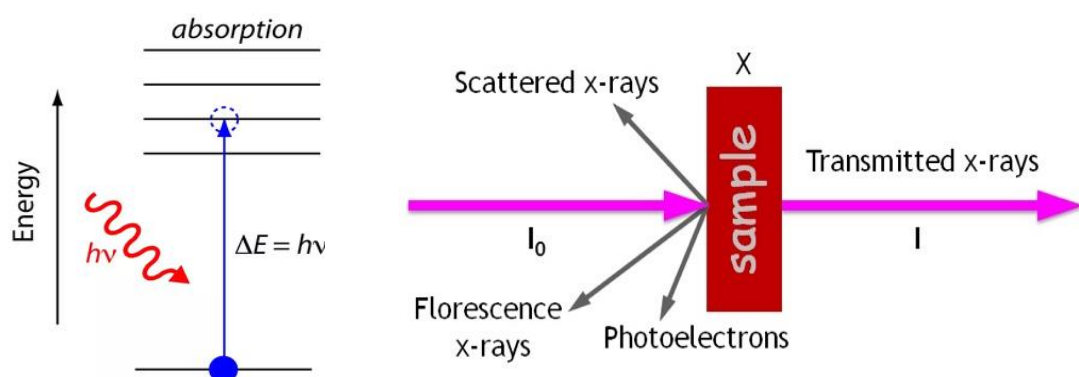


Figure 3.11 The principle for XAS spectra (BL-5.2 SLRI).

XAS with synchrotron radiation is used for studying the local structure of atomic material. This technique can be analysis chemical state, structure of considering atom, bond length, pattern of atom or type of neighboring atoms etc. XAS technique does not destroy the sample and can be applied in many researcher types. The XANES region can be explain the oxidations from edge-shift position and EXAFS explain the local structure.

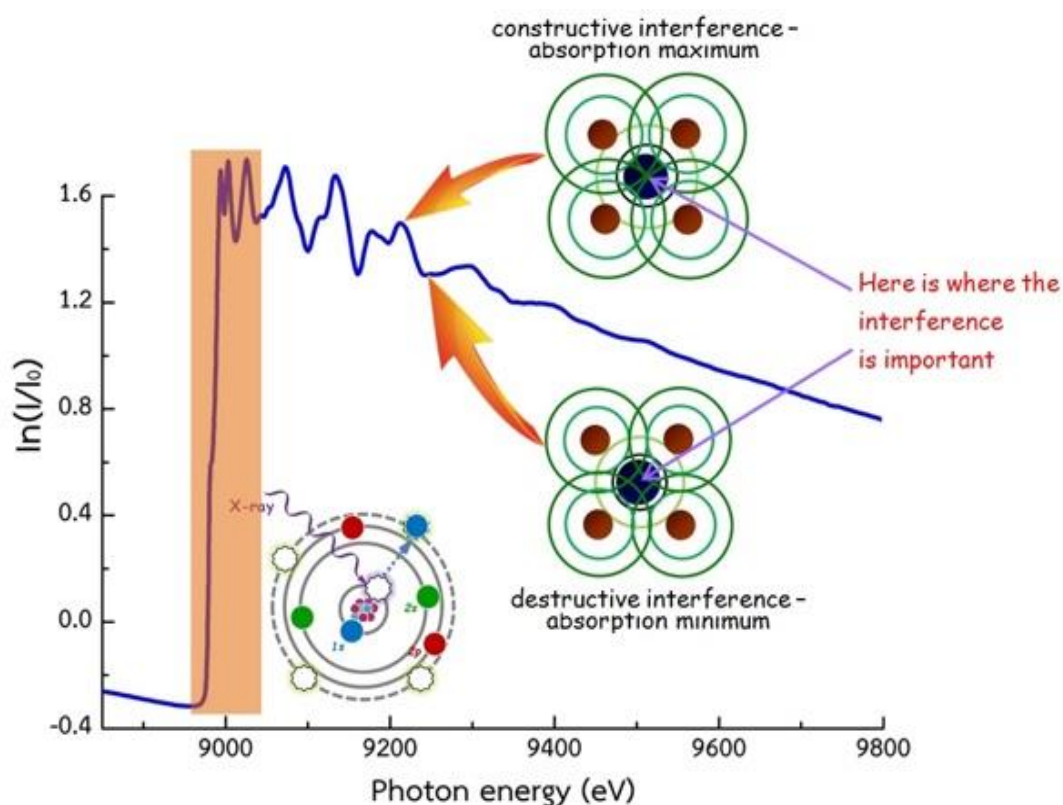


Figure 3.12 Theoretical and algorithm for XANES and EXAFS spectra (BL-5.2 SLRI).

The region very close to the absorption edge is characterized by transitions of the photoelectron to unoccupied bound states. XANES is therefore sensitive to the chemical bonding, exhibiting for example characteristic features for different oxidation states of the absorbing atom. The XANES features are also influenced by strong multiple scattering effects which depend on the three-dimensional geometry of the crystal structure. This provides a means of distinguishing between different crystal phases. Theoretical calculations of the fine structure in this region are complex and the accuracy of such simulations is still limited although significant progress has been made over recent years. Therefore, analysis typically compares the measured spectra

to those of known standards and quantifies the ratios by which these standards are present in the sample using linear combination fitting. Often, the XANES region is also referred to as the near edge X-ray absorption fine structure (NEXAFS) (Schnohr *et al.*, 2015).

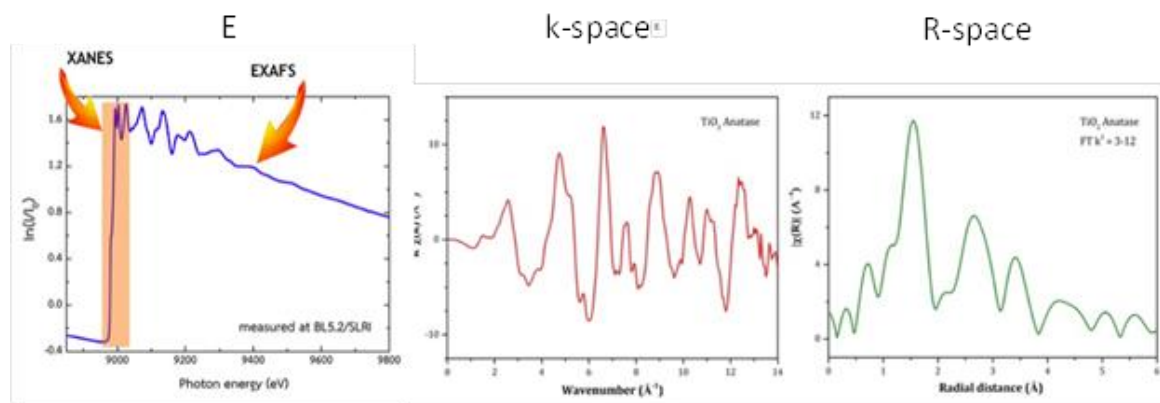


Figure 3.13 Energy range of (a) XANES and EXAFS spectra (b) K-space spectra and (c) R-space spectra (BL-5.2 SLRI).

For photon energies higher than $\sim 30\text{eV}$ above the edge, the photoelectron is promoted to a free or continuum state. EXAFS is thus independent of chemical bonding and depends on the atomic arrangement around the absorber. It contains information about the coordination number, interatomic distances and structural and thermal disorder around a particular atomic species. EXAFS does not require long-range order and is applicable to a wide range of ordered and disordered materials therefore providing a powerful tool for structural analysis. Theoretical calculations of the fine structure in the EXAFS region have also improved enormously during the last two decades and simulations with sufficient accuracy are now available. Nevertheless, the measurement of suitable standards still constitutes an important part of the experimental procedure (Schnohr *et al.*, 2015).

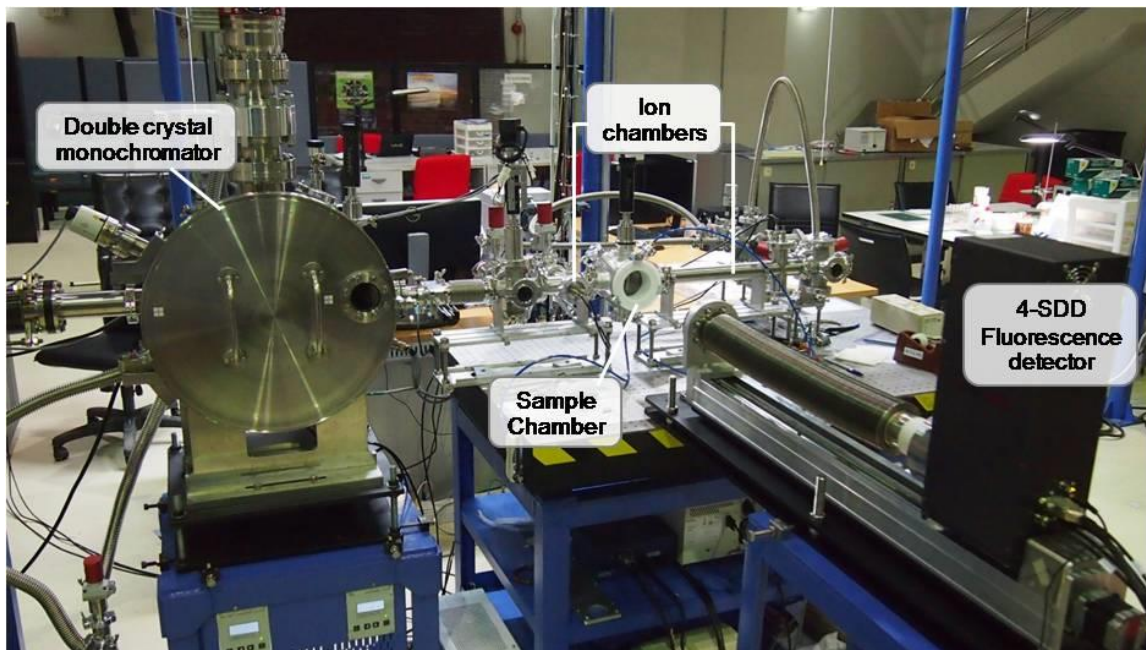


Figure 3.14 SUT-NANOTEC-SLRI beamline setup (BL5.2), SLRI.

3.2.4 UV-Vis-NIR spectroscopy

UV-Vis-NIR spectroscopy is a common, quantitative optical spectroscopic analysis technique which utilizes the absorption of optical radiation for studying the electronic transitions in molecules and solids. When electromagnetic radiations emitted by a light source in ultraviolet ($\lambda = 200-400$ nm), visible ($\lambda = 400-800$ nm) and near infrared ($\lambda = 800-2500$ nm) regions are absorbed by electrons in molecules, they undergo electronic transitions from valance energy level to higher energy levels in which process, the photons are destroyed. This results in optical absorption which depends upon the wavelength of the incident photon. The basic condition for absorption to occur is that the energy of the incident photon should be equal to or greater than the energy bandgap which obeys allowed transition. The absorbance (A) is given by the Beer- Lambert law as

$$A = -\log(I/I_0) = -\log(\%T) \quad (3.4)$$

Where I_0 and I are the intensities of light rays before and after passing through the sample, then the ratio (I/I_0) is called as transmittance.



Figure 3.15 UV-vis spectrophotometer at SUT (<http://cste.sut.ac.th/2014/?p=945>).

3.2.5 Spectroscopic ellipsometry

Spectroscopic ellipsometry, a nondestructive and noncontact optical technique, is an effective method for evaluating the thickness and optical constants of barrier layers during and after deposition. Ellipsometry studies the variations in the state of polarization of light resulting from its reflection off a surface. ellipsometry is sensitive to submonolayer surface covering due to the fact that variations are monitored rather than the absolute intensity of light. As a non-invasive and non-destructive technique, ellipsometry requires just a low-power light source and, as a result, does not interfere with the majority of processes, making it a useful instrument for in situ investigations (Gonçalves, D. *et al.*, 2002). Configuration in spectroscopic ellipsometry and schematic diagram of a polarizer-sample-rotating analyzer ellipsometer are shown in Figure 3.13 and 3.14 respectively. Spectroscopic ellipsometry detects the change in the polarization state of light when it is obliquely reflected off of a thin-film sample, as seen in Figure 3.13. This shift in polarization is represented at every wavelength by two parameters: Δ (phase difference), and Ψ (amplitude ratio). These two parameters are connected to the Fresnel reflection coefficients (r_p and r_s) for the sample according to the formula

$$\rho = \tan \Psi e^{i\Delta} = r_p/r_s \quad (3.5)$$

where r_p and r_s offer information about the optical constants of the sample.

In the case of a phase-modulated ellipsometer, which is the device used to gather the raw data presented below, the observed parameters I_s and I_c are linked to and as follows: $I_s = \sin 2\Psi \sin\Delta$ and $I_c = \sin 2\Psi \cos\Delta$. In order to examine and, or I_s and I_c data, a film structure-representative model must be developed. The sample's attributes, such as thickness and optical constants, may then be determined by using regression analysis to a model of the sample. Spectroscopic ellipsometry is useful for a variety of applications due to the fact that extra study of the optical constants can provide additional information about the sample, such as its composition, crystallinity, band gap, and roughness. Spectroscopic ellipsometry can be conducted either in situ or ex situ, depending on the sample or substance being investigated.

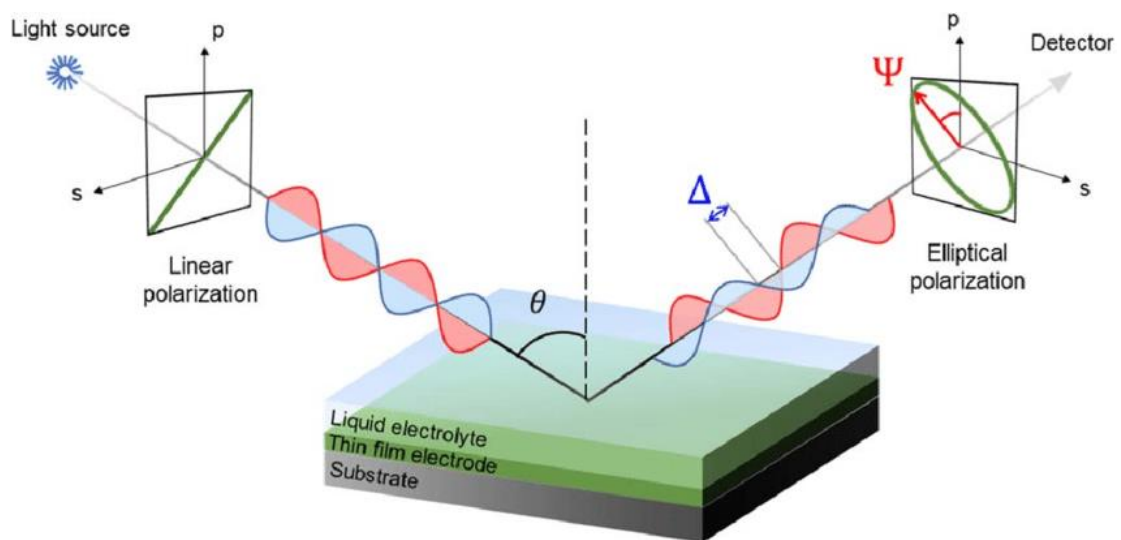


Figure 3.16 Configuration in spectroscopic ellipsometry for a determined incidence angle (θ , degrees). The changes of amplitude (Ψ , degrees) and phase (Δ , degrees) of the reflected elliptically polarized light are measured by the detector (Soult, M.C. *et al.*, 2022).

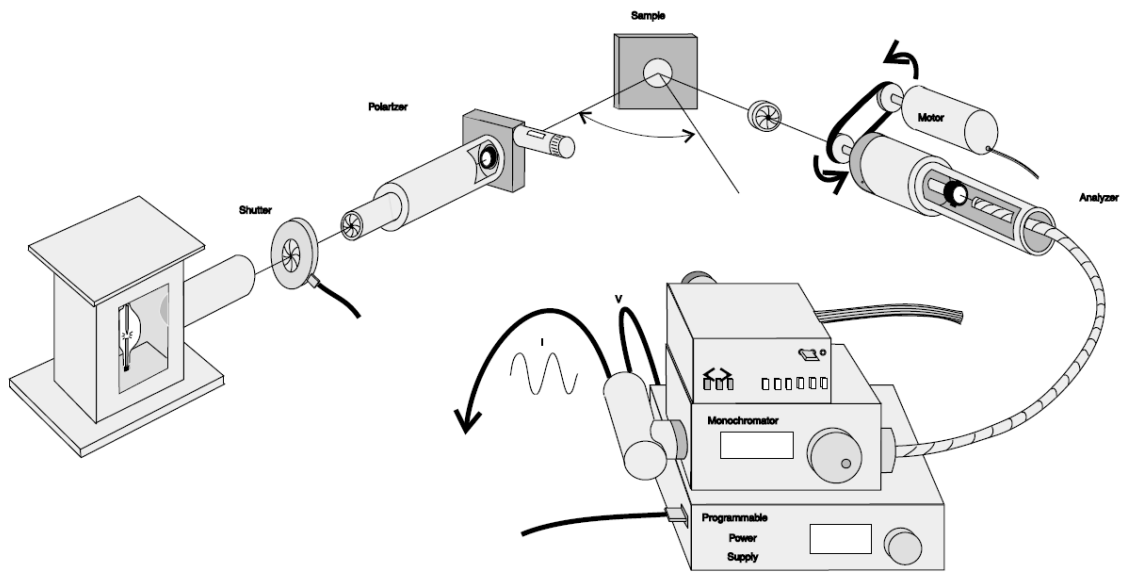


Figure 3.17 Schematic diagram of a polarizer-sample-rotating analyzer ellipsometer (Gonçalves, D. *et al.*, 2002).